Climate Dynamics (2021) 56:3065–3080
https://doi.org/10.1007/s00382-021-05636-9

The inter-annual variations of the significant wave height in the Western North Pacific and South China Sea region

Shaotian Li[1,3,4] · Yineng Li[1,2,3,4] · Shiqiu Peng[1,2,3] · Zhanhui Qi[5]

Received: 23 March 2020 / Accepted: 4 January 2021 / Published online: 19 January 2021

Abstract
The spatio-temporal variations of the significant wave height (SWH) in the Western North Pacific and South China Sea (WNP-SCS) region, as well as their driving mechanisms, are investigated based on the long-term (1981–2014) simulation by a coupled ocean–atmosphere model and a WAVEWATCH III model. The Empirical Orthogonal Function modes of SWH anomalies show different patterns in the cold and warm seasons. In winter, the first mode (explaining 40.63% of the variance) shows a monopole pattern with large loadings lying in SCS and the WNP to the east of the Philippine Islands, which is primarily associated with the El Niño-Southern Oscillation (ENSO) on inter-annual time scales. The second mode (explaining 19.62% of the variance) shows a dipole pattern with negative loadings in the northeastern SCS and positive loadings to the east of Japan, which is prominently connected with the intensity variation and longitudinal shift of Aleutian Low on decadal time scales. In summer, the first leading mode (explaining 73.47% of the variance) presents large loadings located mainly in the WNP region between 10° N and 30° N and secondarily in the central SCS, which is associated with the ENSO-affected tropical cyclone activities and South China Sea summer monsoon, respectively.

Keywords Significant wave height · Empirical orthogonal function · Monsoon · Tropical cyclones · Aleutian low · WAEWATCH III

1 Introduction

The ocean surface waves play an important role in the oceanic variability. The surface wind and wave help to control the energy flux between atmosphere and ocean (Semedo et al. 2011; Yan et al. 2020) and the upper ocean mixing (Craig and Banner 1994; Li et al. 2014; Young et al. 2011). They further influence climate change and wave energy evaluation and development (Liu et al. 2017; Zheng et al. 2013, 2019). The IPCC reports suggested that estimation of changes in wave height characteristics was necessary for estimating the impact of climate change on coastal erosion, shifts of storm tracks and increases of storm frequency and intensity (Bernstein et al. 2008). Additionally, the long-term variations of ocean surface waves are of importance to shipping, military activities and coastal interests in practical applications (Young and Babanin 2020). Therefore, it is crucial to understand the spatial patterns and temporal variations of ocean surface waves as well as the associated dynamical mechanisms.

The western North Pacific (WNP) and South China Sea (SCS) region are one of the regions of the most

✉ Yineng Li
lyneng@scsio.ac.cn

✉ Shiqiu Peng
speng@scsio.ac.cn

1 State Key Laboratory of Tropical Oceanography, South China Sea Institute of Oceanology, Chinese Academy of Sciences, Guangzhou 511458, China

2 Key Laboratory of Science and Technology on Operational Oceanography, Chinese Academy of Sciences, Guangzhou 511458, China

3 Southern Marine Science and Engineering Guangdong Laboratory (Guangzhou), Guangzhou 511458, China

4 Institution of South China Sea Ecology and Environmental Engineering, Chinese Academy of Sciences, Guangzhou 511458, China

5 National Ocean Technology Center, No. 219 Jieyuanxidao Road, Nankai District, Tianjin 300112, China

frequent human activities as well as complex atmospheric processes, such as monsoon, subtropical high, tropical cyclones (TCs), etc. (Chu 2004; Wang et al. 2010, 2013). The complex atmospheric conditions result in significant variations of ocean surface waves on different time scales. In this manner, it is necessary to investigate the characteristics of the inter-annual or even decadal variations of ocean surface waves in this region.

When considering the long-term variations of the wave height in the WNP-SCS region, previous works mainly focused on the extreme wave height obtained through statistical derivation from observations or reanalysis datasets. The long-term variations of the extreme wave height in the WNP or SCS are related to the Aleutian Low (AL) activities and the frequency of extreme cyclones (e.g. Graham and Diaz 2001; Sasaki et al. 2005, 2006; Sasaki and Toshiyuki 2007; Wang and Swail 2001). In addition, there is an increasing long-term trend of the extreme wave height in this region (e.g. Osinowo et al. 2016; Young et al. 2012, 2011).

Comparing to the extreme wave height, the significant wave height (SWH) is used as a well-defined and standardized statistic to denote the characteristic height of the random waves in a sea state, which is well correlated with the characteristic wave height observed visually by experienced observers (Holthuijsen 2007; Tolman 2009). It is more suitable for investigating the long-term variations of the wave climate and the corresponding physical mechanisms. Previous studies connected the inter-annual variation of the SWH with the El Niño-Southern Oscillation (ENSO) events in SCS or WNP (e.g. Si and Kubota 2006; Mirzaei et al. 2013; Zhu et al. 2015). The impact of ENSO on the SWH anomalies in wintertime over the SCS is bridged by the Pacific-East Asian teleconnection in the lower troposphere (Zhu et al. 2015). In addition, Jiang et al. (2018) investigated the inter-annual variations of the SWH in the Northern SCS and related the variations to the El Niño events and typhoon activities. However, most of these studies focused on the inter-annual variations of the SWH in a certain part of the WNP-SCS region, such as SCS or northern SCS. Additionally, the long-term variations of the SWH and the corresponding physical mechanisms in the whole WNP-SCS region have not been well demonstrated. Therefore, we aim to clarify this issue in this study through a 34-year (1981–2014) wave simulation using the WAVEWATCH III model, focusing on the canonical boreal winter (December to February in the next year, DJF) and summer (June to August, JJA) seasons.

This paper is arranged as follows: Sect. 2 gives a description of the data, model configuration and validation. The spatio-temporal variations of the SWH and their driving mechanisms are presented in Sect. 3, followed by a discussion in Sect. 4. A summary is given in Sect. 5.

2 Methods and data

In this study, we aim to investigate the primary spatial and temporal variations of the SWH in the WNP-SCS region and identify the corresponding driving mechanisms by comparing the leading Empirical Orthogonal Function (EOF) modes with the climate events. For this objective, a long-term wind and wave dataset during 1981–2014 is generated by a coupled ocean–atmosphere model (COAM) and a WAVEWATCH III model over the WNP-SCS region. A brief introduction of the COAM and WAVEWATCH III model, as well as the associated climate indices, is given as follows.

2.1 Coupled ocean–atmosphere model

To obtain more accurate wind, we build up a COAM, which consists of a Weather Research and Forecasting (WRF) model and a Princeton Ocean Model (POM). WRF is double-nested with the inner domain coupled with POM through the Ocean Atmosphere Sea Ice Soil (OASIS) coupler (Valcke 2013). In the COAM, WRF provides the sensible heat flux, latent heat flux and solar radiation, while POM produces the sea surface temperature (SST). The wind stress is computed using the 10-m wind from WRF and the sea surface current from POM. Comparing with the uncoupled WRF, the coupled model can produce more detailed variations, such as the diurnal variation (Li et al. 2014; Luo et al. 2005; Palmer et al. 2004). The COAM covers the WNP-SCS region and parts of Eastern Indian Ocean (78° E–150° E, 22° S–41.5° N, Fig. 1) with resolutions of 1/6° for POM and 27 km for the inner region of WRF, respectively.

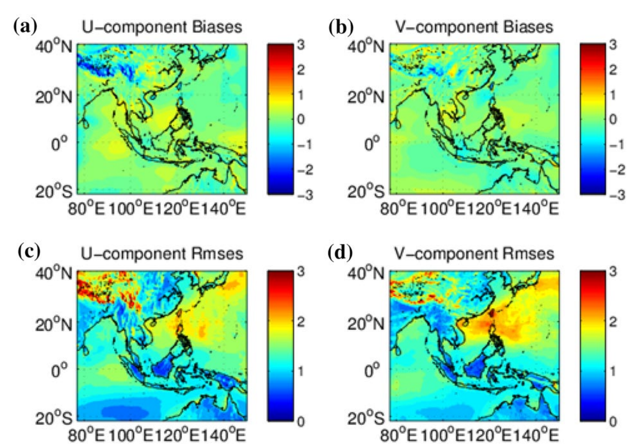

Fig. 1 Maps of mean absolute errors (**a**, u-component; **b**, v-component) and variances of the mean absolute error (**c**, u-component; **d**, v-component) between the modelled wind and the Cross-Calibrated Multi-Platform wind vector analysis during the period of 1981–2010

For WRF, the National Centers for Environmental Prediction (NCEP) reanalysis is used as the initial and boundary conditions, including the 2.5°×2.5° data from 1980 to 1997 and FNL (final) 1°×1° data from 1997 to 2014. The model is re-initialized every 12 h and the results of 7–18 h are used. Even though the data assimilation is applied, the winds around the TCs in most of the wind reanalysis are underestimated due to the inadequate horizontal resolution (Alves et al. 2017; Cavaleri and Sclavo 2006; Hodges et al. 2017; Murakami 2014; Signell et al. 2005; Swail and Cox 2000). Forced by the underestimated peak wind speed, the wave height is systematically underestimated at a high sea state. Generally, the reanalysis data perform better in the areas far away from the cyclone center, while the empirical TC model has high accuracy in reproducing the wind field near the cyclone center (Lin and Chavas 2012; Young 2017). Therefore, we superpose the empirical wind field from the Holland model (Holland 1980) on the modelled results (Jiang et al. 2018; Kalourazi et al. 2020; Pan et al. 2016). The Holland model is calculated using the best track data from the Joint Typhoon Warning Center (JTWC).

For the ocean model, the World Ocean Atlas 2013 (WOA13) dataset is used as the initial field, while the climatological NCEP reanalysis and Simple Ocean Data Assimilation (SODA) data are used as sea surface forcing and boundary conditions during the 20-year spin-up, respectively. Then, POM is coupled with WRF and integrated forward.

2.2 Wave spectrum model and Dataset

The 10-m wind, sea surface current and water level produced by the COAM are adopted to force the WAVEWATCH III model. The wave model covers the same region as the COAM with a spatial resolution of 0.25°. The gridded bathymetric data for the wave model comes from the General Bathymetric Chart of the Oceans (GEBCO) dataset at 30 arc-second intervals (www.gebco.net). The wave parameters, consisting of SWH, mean wave length (LMN), mean wave period (TMN) and mean wave direction (DIRMN), are output at 6-h intervals from 1981 to 2014.

2.3 Model validation

The wind data are validated against the Cross-Calibrated Multi-Platform (CCMP) wind vector analysis (Atlas et al. 2011). In most of the region, the mean absolute errors (MAEs) of wind components are less than 1.0 m/s with the exception in the marginal area of Tibet Plateau (Fig. 1a and b). In terms of the root-mean-square error (RMSE) (Fig. 1c and d), large errors (> 2.0 m/s) are found in the marginal area of Tibet Plateau and the tropical WNP region where TCs pass by. The CCMP wind usually underestimates the wind speed around the TC-core (Pan et al. 2016). Therefore, the positive biases in the tropical WNP where the TCs pass by mainly come from the aforementioned wind reconstruction using the Holland model (Holland 1980). Moreover, the European Centre for Medium-Range Weather Forecasts (ECMWF) Reanalysis V5 (ERA5), which has been proven reliable with a substantial improvement compared to the ERA-Interim (Belmonte Rivas and Stoffelen 2019; Bruno et al. 2020; Mahmoodi et al. 2019), is adopted to validate the long-term trends of the modelled results. ERA5 is provided at hourly intervals and in a horizontal resolution of 0.25° for atmospheric variables (0.5° for ocean surface wave parameters) (Hersbach et al. 2020). The correlation analysis is applied to the daily mean wind speed obtained from the COAM and ERA5 during 2006–2013. The correlation coefficients (CC) are greater than 0.90 over most of the WNP-SCS region (Fig. 2a), indicating that the wind of the COAM has a similar variation with that of ERA5.

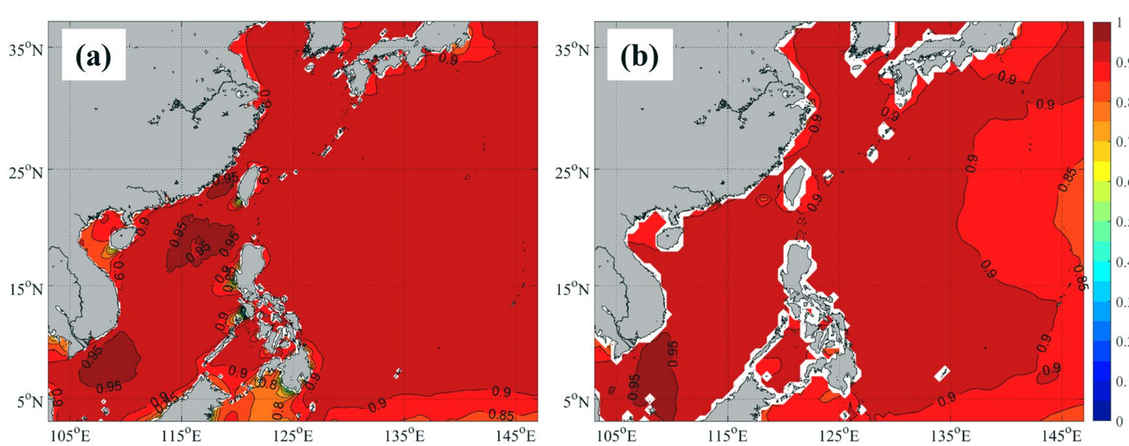

Fig. 2 The distribution of the correlation coefficients between the ERA5 reanalysis and the model outputs of **a** wind speed and **b** significant wave height during 2006–2013

Due to the limited availability of observations, only two buoys to the east of Philippine Islands are used for the wave model validation in this study. The time series cover from 10/29/2013 to 11/02/2013 (Buoy01) and from 28/10/2013 to 11/11/2013 (Buoy02). During this period, typhoon 'Krosa' (201,329) and super typhoon 'Haiyan' (201,330) passed by the Buoys. Referring to Reistad et al. (2011) and Zheng and Li (2015), the biases, MAEs, RMSE, normalized RMSE (NRMSE), scatter Index (SI) and CCs of the SWH from our model and ERA5 are calculated and presented in Fig. 3 and Table 1. The CCs between the modelled results and observed SWH are 0.97 and 0.95 for Buoy01 and Buoy02, respectively, which are similar to those of ERA5. It indicates the model describes the temporal trend well. The MAEs (RMSEs) of the modelled SWH against the buoy01 and buoy02 are 0.27 m (0.36 m) and 0.24 m (0.34 m) with low scatter indices (7.66–11.25%), respectively. They are smaller than those of ERA5 with the magnitude of 0.827 m (0.649 m) and 0.599 m (0.460), respectively. According to the previous studies (Caires et al. 2004; Si and Kubota 2006; Reistad et al. 2011; Sasaki et al. 2005; Sasaki and Toshiyuki 2007; Swail and Cox 2000), the ranges of the bias, MAEs, RMSE, SI and CCs of the wave products or reanalysis are − 0.59 to 0.62 m, 0.28–0.48 m, 0.15–1.20 m, 20.8–30.0% and 0.80–0.97, respectively. The error statistics of the modelled SWH are in an acceptable range. In particular, the CCs between the daily mean modelled SWH and ERA5 in 2006–2013 are greater than 0.85 over most of the WNP-SCS region (Fig. 2b). Therefore, the wave simulation is reliable for further analysis.

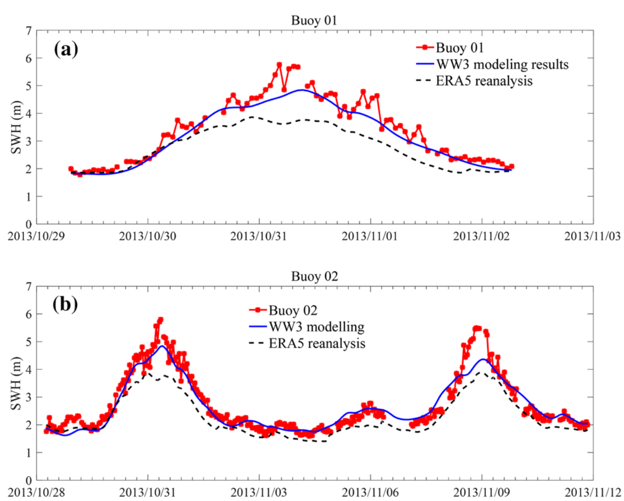

Fig. 3 The time series of the significant wave height (unit: m) from the buoy observations, model outputs and ERA5 reanalysis during the observation time of **a** Buoy 01 and **b** Buoy 02. The corresponding error statistics are presented in Table 1

2.4 Climate indices

Four climate indices are adopted in this study to explore the relationship between the SWH variations and climate variabilities, including Ocean Niño Index (ONI), Northern Pacific Index (NPI), Accumulated Cyclone Energy (ACE) index and South China Sea summer monsoon (SCSSM) index.

2.4.1 Ocean Niño Index

The ONI is the primary indicator used by National Oceanic and Atmospheric Administration (NOAA) to monitor ENSO. It is defined as the three months running mean of the SST anomalies in the Niño 3.4 region (5° N–5° S, 120°–170° W) from NOAA Extended Reconstructed Sea Surface Temperature V5 (ERSST.V5), based on centered 30-year base periods updated every 5 years. Positive (negative) ONI signifies a warming (cooling) event in the equatorial eastern-central Pacific. The index is obtained from NOAA Climate Prediction Center (CPC) (https://origin.cpc.ncep.noaa.gov/products/analysis_monitoring/ensostuff/ONI_v5.php). The cold and warm events are defined when the threshold ± 0.5 °C is met for a minimum of 5 consecutive over-lapping seasons, referred to Wu and Li (2014).

2.4.2 North Pacific Index

The NPI also comes from NOAA CPC (https://www.psl.noaa.gov/data/climateindices/list/). It is defined to describe the variations of the AL intensity, the area-weighted sea level pressure over the region 30° N–65° N, 160° E–140° W (Trenberth and Hurrell 1994). It is highly correlated with the 500 hPa Pacific/North America (PNA) index (Sugimoto and Hanawa 2009; Wallace and Gutzler 1981). Negative (positive) NPI means the strengthening (weakening) AL intensity. The time series is monthly, and the averages in JJA and DJF are used as the summer and winter indices, respectively.

Table 1 Comparison between the modelled SWH (ERA5 wave reanalysis) and buoys observations

Dataset	Buoy	Bias (m)	MAEs (m)	RMSE (m)	NRMSE	SI (%)	CC
Modelled results	Buoy01	− 0.232	0.267	0.359	0.100	7.66	0.97
	Buoy02	− 0.068	0.243	0.338	0.115	11.25	0.95
ERA5	Buoy01	− 0.638	0.649	0.827	0.231	14.69	0.93
	Buoy02	− 0.455	0.460	0.599	0.203	13.24	0.96

2.4.3 Accumulated cyclone energy

Referring to Bell et al. (2000), the ACE index is defined as the square of the maximum wind speed summed over the lifetime of a TC within the region 10° N–30° N, 110° E–150° E.

$$ACE = 10^{-4} \sum v_{\max}^2 \tag{1}$$

where $v_{\max}$ is the estimated maximum sustained velocity (in knots) of the intense TCs (wind speed ≥ 35 knots) at 6-h intervals. It is related to storm kinetic energy, whose unit is 10^4 kn^2. It takes into account the number, intensities and lifetimes of the TCs and is appropriate for indexing the effect of tropical cyclones on climate process (Camargo and Sobel 2005; Chan 2016). The seasonal ACE is the sum of the ACEs for each TC in certain season. In this study, the wind hindcast from the COAM is employed to calculate the ACE index.

2.4.4 South China Sea Summer Monsoon Index

The SCSSM index is defined as an area-averaged seasonally (June to September) dynamical normalized seasonality (DNS) at 925 hPa within the SCS monsoon domain (0°–25° N, 100°–125° E) (Li and Zeng 2002, 2003). The index we obtained from the website (http://ljp.gcess.cn/dct/page/65578) is monthly, and only the data in JJA are used for consistency.

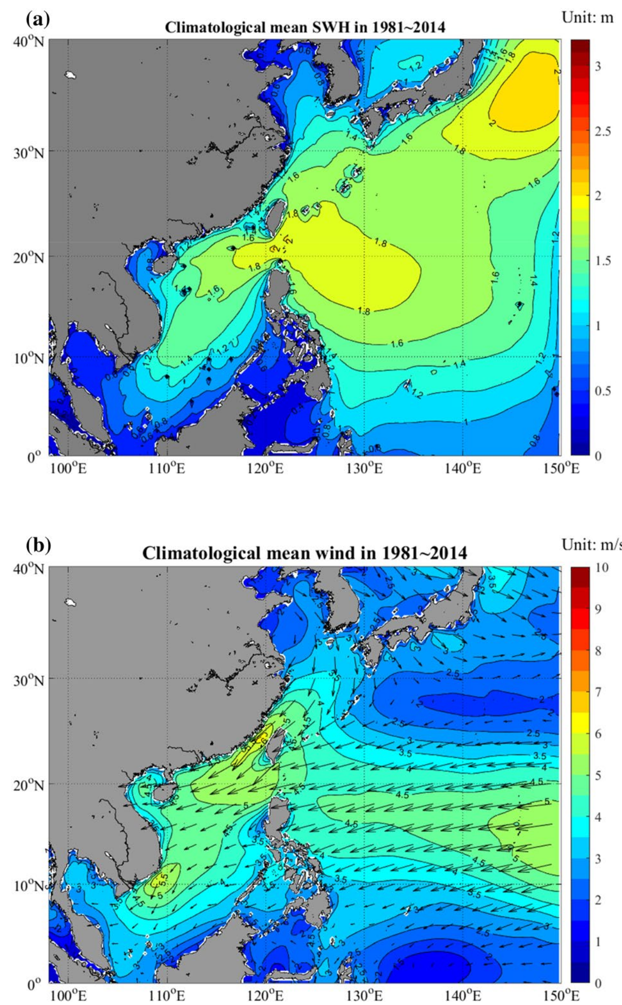

Fig. 4 The climatological annual mean of the **a** significant wave height (SWH) and **b** 10-m height wind in the WNP-SCS region during the period of 1981–2014

3 Results and analysis

3.1 Overall spatial distribution and temporal trend

The annual mean SWH during the 1981–2014 period (Fig. 4a) shows a dipole pattern, in which the high SWH with the magnitude greater than 1.8 m occurs to the east of Japan between 30° N and 40° N and around the Luzon Strait-Philippines Island. This pattern is similar to that of Zheng and Li (2015) but with a slightly larger magnitude. It might be attributed to the wind reconstruction using the Holland model (Holland 1980). The annual mean wind shows westerly to the east of Japan, easterly in the low-latitude WNP (10° N–23° N) and northeasterly in SCS (Fig. 4b). The strongest wind is located in Taiwan Strait and the southeast of Vietnam. As a result, the wave energy propagates into SCS through Luzon Strait.

Figure 5a presents the standard deviation of the annual mean SWH. A region of prominent SWH variation can be seen in the northern SCS and the east of the Philippine Islands. Thus, we just discuss the long-term trends of the SWH and wind speed in the region of 98° E–150° E and 10° N–23° N. The annual mean trends of the SWH and wind speed are analyzed using the linear regression method, which passes the reliability test of 95%. The time series of the annual mean SWH shows significant inter-annual variation and a slightly increasing trend (0.0013 m/year) (Fig. 5b), which is much smaller than that (0.0152 m/year) of Zheng and Li (2015). A close look finds that, the SWH decreases with the slope of – 0.0116 m/year from 1981 to 1998, but increases with the rate of 0.0093 m/year after 1998. This non-monotonical trend is consistent with that in Osinowo et al. (2016) and Zhu et al. (2015). Similarly, the wind speed decreases before 1998 and increases from 1999 to 2014 (Fig. 5c). This phase shift of the SWH and wind speed in the mid-1990s in the WNP-SCS region is associated with the impact of Pacific Decadal Oscillation (PDO) or the variation of the AL intensity on the East Asian

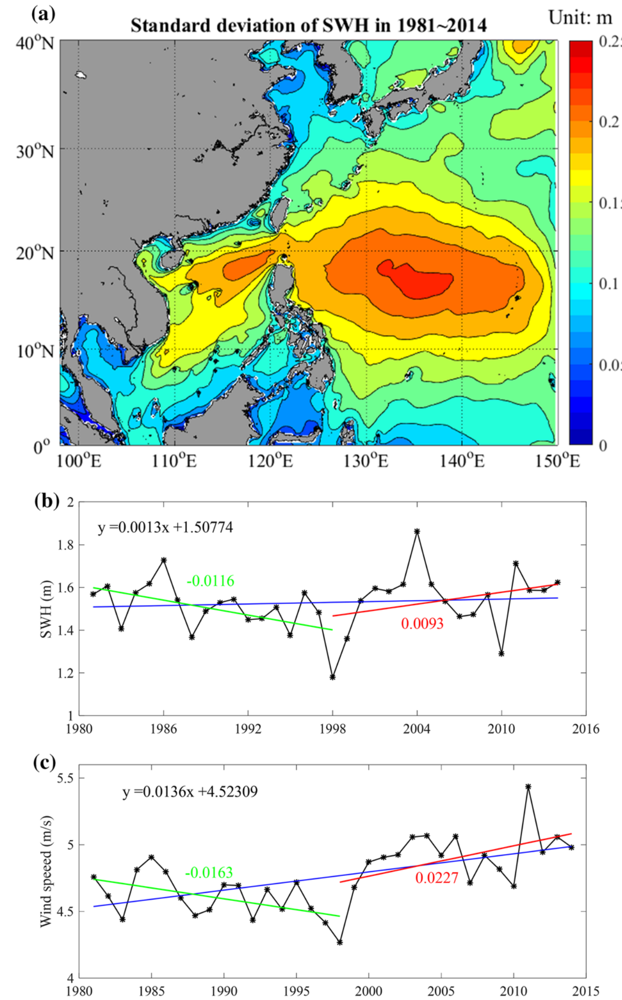

Fig. 5 **a** The standard deviation (unit: m), time series of the annual mean (**b**) significant wave height (SWH, unit: m) and **c** wind speed (unit: m/s) in the region of 98–150° E, 10–23° N. The contour level is 0.02 m in (**a**)

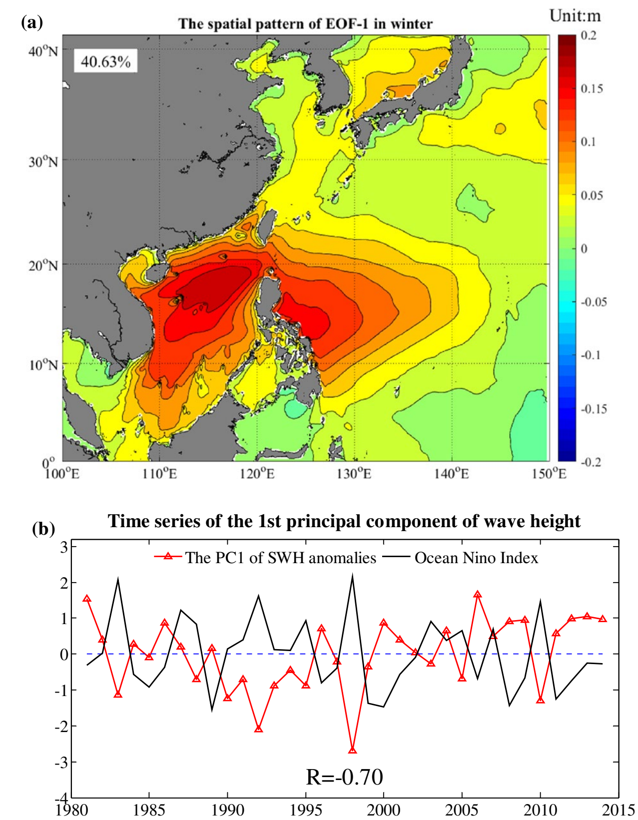

Fig. 6 **a** The spatial pattern and **b** corresponding principle components of the first mode of the significant wave height anomalies overlaid with the Ocean Niño index in the WNP-SCS region in winter (DJF). Both time series are normalized. The contour level is 0.02 m

Winter Monsoon (EAWM) (Schneider and Cornuelle 2005; Zhu et al. 2015).

3.2 Inter-annual variations of the ocean waves

In this section, the EOF analysis is employed to extract the dominant patterns and their associated time coefficient for analyzing the inter-annual variations of the SWH in winter and summer. The analysis is conducted after subtracting the climatological monthly mean from the raw data. All the time series of principle components (PCs) and climate indices are normalized to have unit variance. The significance of correlations is determined using the Student *t*-test.

3.2.1 Variations in winter (DJF)

In winter (DJF), the first two leading modes of EOFs explain about 60.05% of the total variance, with 40.63% for the first mode (EOF-1) and 19.62% for the second mode (EOF-2), respectively. Referring to Fang et al. (2006), we only discuss the first two modes, whose contributions exceed 15%, in the following. The spatial pattern of EOF-1 (Fig. 6a) shows a monopole pattern with maximum loadings lying in the northern SCS and to the east of Philippine Islands (5° N–23° N). This principal component (PC-1, the time series of EOF-1) has a pronounced negative correlation with the ONI in DJF (the peak season of ENSO), whose correlation coefficient is up to -0.70 above the 99% confidence level (Fig. 6b). Four troughs of the PC-1 correspond well to the strong El Niño events of 1982–1983, 1991–1992, 1997–1998 and 2009–2010 when the below-normal SWH occurs in the northern SCS and the WNP region around Philippine Islands; several peaks of the PC-1 correspond well to the strong La Niña events of 1984–1985, 1988–1989, 1998–1999, 1999–2000, 2007–2008 and 2010–2011 when the above-normal SWH occurs. The results imply that the warming (cooling) events in the equatorial eastern-central Pacific weaken (intensify) the wave height in SCS and the east of Philippine Islands. We further check the wind anomalies in DJF of the strong El Niño years during 1981–2014, i.e., 1982–1983, 1986–1987, 1991–1992, 1997–1998, 2002–2003 and 2009–2010. As shown in Fig. 7a, there is an anomalous anticyclone wind over SCS and tropical WNP, which weakens the northeasterly monsoon and then the SWH. In contrast, the northeasterly monsoon, as well as SWH, is intensified by the cyclone anomalies over the Philippine Sea during the strong La Niña events (Fig. 7b). The results are similar to those of previous studies (e.g. Wang et al. 2000; Wang and Zhang 2002). The warming (cooling) in the equatorial eastern-central Pacific leads to the weaker (stronger) than normal northeasterly monsoon through the lower tropospheric anticyclone (cyclone) over the Philippine Sea. As a result, the lower (higher) SWH occurs in SCS and the WNP to the east of Philippine Islands. It indicates that ENSO is the primary forcing processes of the SWH variations over the WNP-SCS region in winter.

Regarding to the EOF-2 (explaining 19.62% of the total variance) in winter, it shows a northeast-southwest dipole pattern with the center of large negative loadings in the northeastern SCS and large positive loadings located to the east of Japan (Fig. 8a). After a 9-year Gauss filtering, the filtered PC-2 is found to be prominently correlated with the NPI (R = − 0.85) during the period of 1984–2011 (Fig. 8b), exceeding the 99% confidence level. As mentioned above (Sect. 2.4), negative (positive) NPI means the strengthening (weakening) AL intensity, accompanying with the longitudinal (east–west) movement of the AL center (Hanawa et al. 1989; Sugimoto and Hanawa 2009). To further investigate the relationship between the PC-2 and the AL activities, the

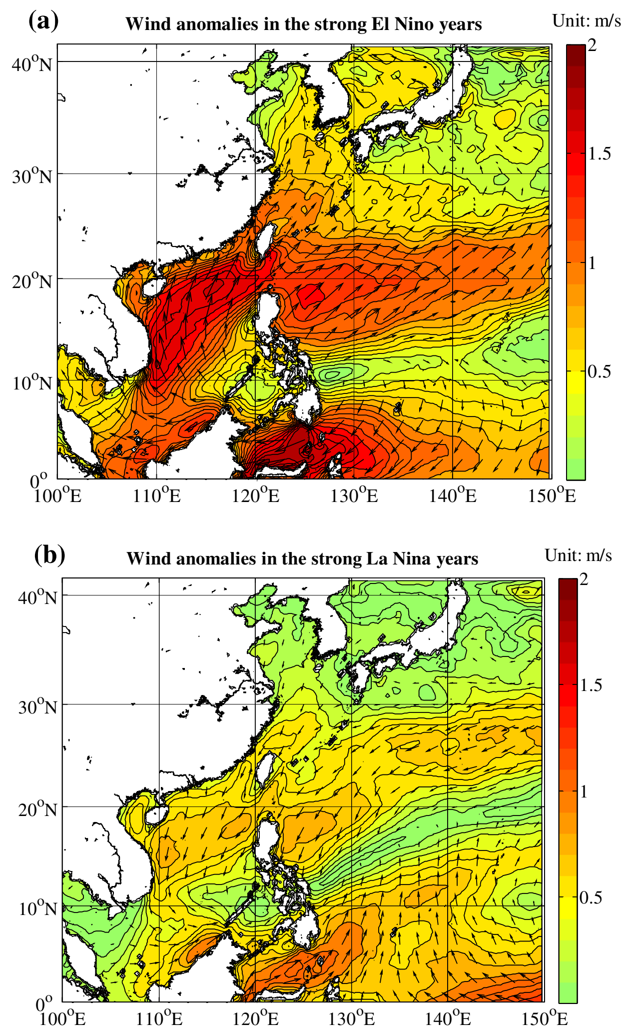

Fig. 7 Composite wind anomalies (unit: m/s) against the climatological mean in winter (DJF) of **a** the strong El Niño years (1982–1983, 1986–1987, 1991–1992, 1997–1998, 2002–2003 and 2009–2010) and **b** the strong La Niña years (1984–1985, 1988–1989, 1998–1999, 1999–2000, 2007–2008 and 2010–2011). The contour means the wind speed anomalies with an interval of 0.1 m/s; the vector is the direction of the wind anomalies

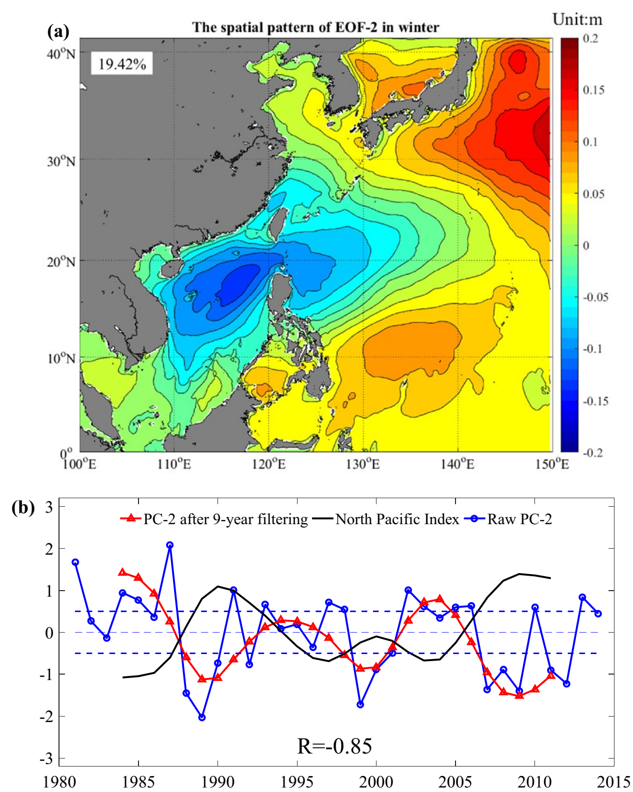

Fig. 8 **a** The spatial pattern and **b** corresponding principle components (PC) of the second mode of the significant wave height anomalies in the WNP-SCS region overlaid with the North Pacific Index (NPI) in winter (DJF) during the period of 1984–2011. Blue line with circle in **b** is the raw time series of the second mode without time filtering; dot lines stand for ± 0.5δ of the time series of the NPI with no filtering; R = − 0.85 in **b** is the correlation coefficient between the filtered PC-2 and NPI; all the time series are normalized. The contour level is 0.02 m in **a**

strong (weak) AL years are selected with the normalized NPI exceeding the magnitude of a half standard deviation (±0.5δ) (see Fig. 8b). Subsequently, we compare the composite wind in the years of strong AL (1981, 1983, 1986, 1987, 1992, 1995, 1998, 2001, 2003, 2004 and 2010) with the climatological wind, and wind anomalies are presented in Fig. 9a. With the eastward shift of the AL center, the AL intensity strengthens, and the westerly wind intensifies in the subtropical WNP (Sugimoto and Hanawa 2009; Trenberth and Hurrell 1994). On the other hand, the northeasterly monsoon in the low-latitude WNP-SCS region weakens (Chen et al. 2014; Si and Kubota 2006), along with the occurrence of the anticyclone over the Philippine Islands. As a result, the SWH is higher than normal in the region to the east of Japan, while the one in the northern SCS and the east of Luzon Strait becomes lower (Fig. 8a). The anomalies of the wind and SWH reverse in the years of weak AL (1982, 1985, 1989, 1990, 1993, 1994, 1999, 2000, 2002, 2008, 2009, 2011 and 2013) (Fig. 9b). These results indicate that the SWH variations in the WNP-SCS region are influenced by the intensity variations and longitudinal shift of the AL on decadal time scales.

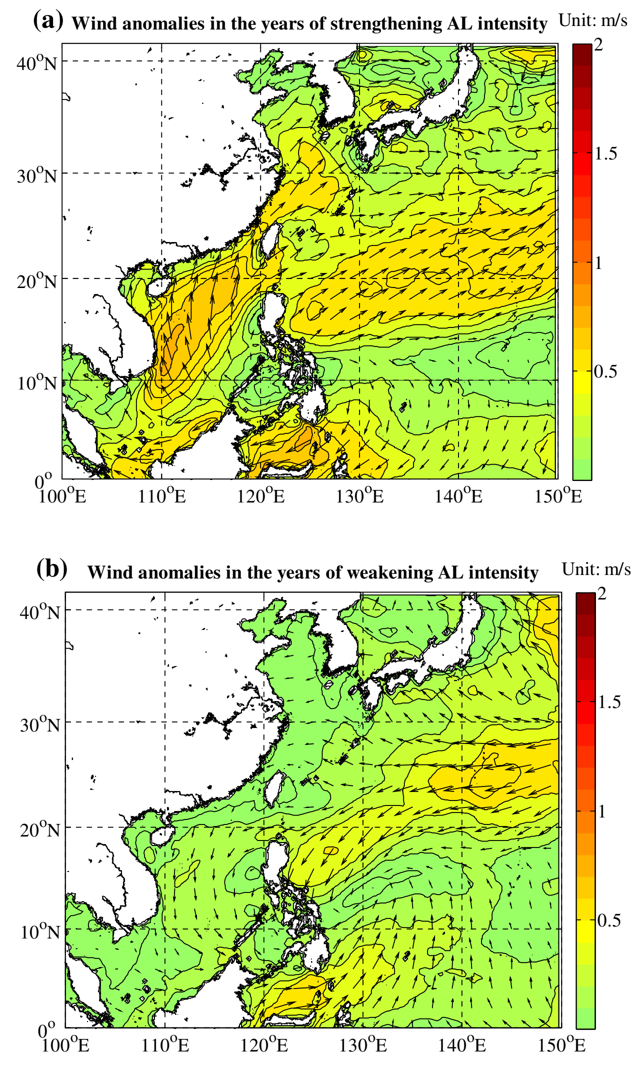

Fig. 9 Composite wind anomalies (unit: m/s) against the climatological mean in winter (DJF) in the years of **a** strengthening Aleutian Low (AL) intensity (extreme negative NPI) (1981, 1983, 1986, 1987, 1992, 1995, 1998, 2001, 2003, 2004 and 2010) and **b** weakening AL intensity (extreme positive NPI) (1982, 1985, 1989, 1990, 1993, 1994, 1999, 2000, 2002, 2008, 2009, 2011 and 2013). The contours with an interval of 0.1 m/s denote the wind speed anomalies, and the vectors are the direction of the wind anomalies

3.2.2 Variations in summer (JJA)

In summer (JJA), the EOF-1 accounts for about 73.47% of the total variance (in Fig. 10a), while the EOF-2 only accounts for 9.67%. Therefore, we only discuss the EOF-1. The spatial pattern of the EOF-1 shows large positive loadings in the tropical WNP region (10° N–30° N), where there is a frequent occurrence of TCs (Chan 2000, 2016; Chu 2004). It implies that the EOF-1 represents the impact of TC activities on the SWH variations, which induces not only high wind waves near the TC center, but also strong swells propagating to a far region in the open ocean. The ACE index is generally adopted to represent the storm kinetic energy (Bell et al. 2000; Camargo and Sobel 2005). The spatial pattern of the EOF-1 is similar to that of the summation of ACE in JJA during the period of 1981–2014 (Fig. 11a), in which the salient region is located in the tropical WNP of high accidence of intense TCs (Fig. 11b). The PC-1 is prominently associated with the ACE index in JJA on interannual time scales as well, with the correlation coefficient up to 0.87 exceeding the 99% confidence level (Fig. 10b). It indicates that the PC-1 is notably characterized by the TC activities. In addition, we notice that the PC-1 is also statistically significantly correlated with the SCSSM index and ONI in JJA, whose correlation coefficients are R = 0.66 and R = 0.58, respectively, above the 99% confidence level (Fig. 10c and Table 2). Therefore, the EOF-1 in summer involves the SWH variations related to different forcing processes, such as TCs and SCSSM.

Monahan et al. (2009) indicated that components cannot be separated by the EOF analysis if they are not completely orthogonal. Therefore, we apply the rotated EOF (REOF) analysis to distinguish the impacts of TCs and monsoon (Chen et al. 2014; Lian and Chen 2012). The first mode of the rotated EOFs (REOF-1) (Fig. 12a) explains about 50.68% of the total variance. Its spatial pattern is similar to that of the EOF-1, except that the center of large loadings is only located in the tropical WNP region and moves southeastward. The time series of the REOF-1 is significantly correlated with the ACE index in JJA with the correlation coefficient of R = 0.73 exceeding the 99% confidence level (Fig. 12b). It confirms that the SWH variations in the

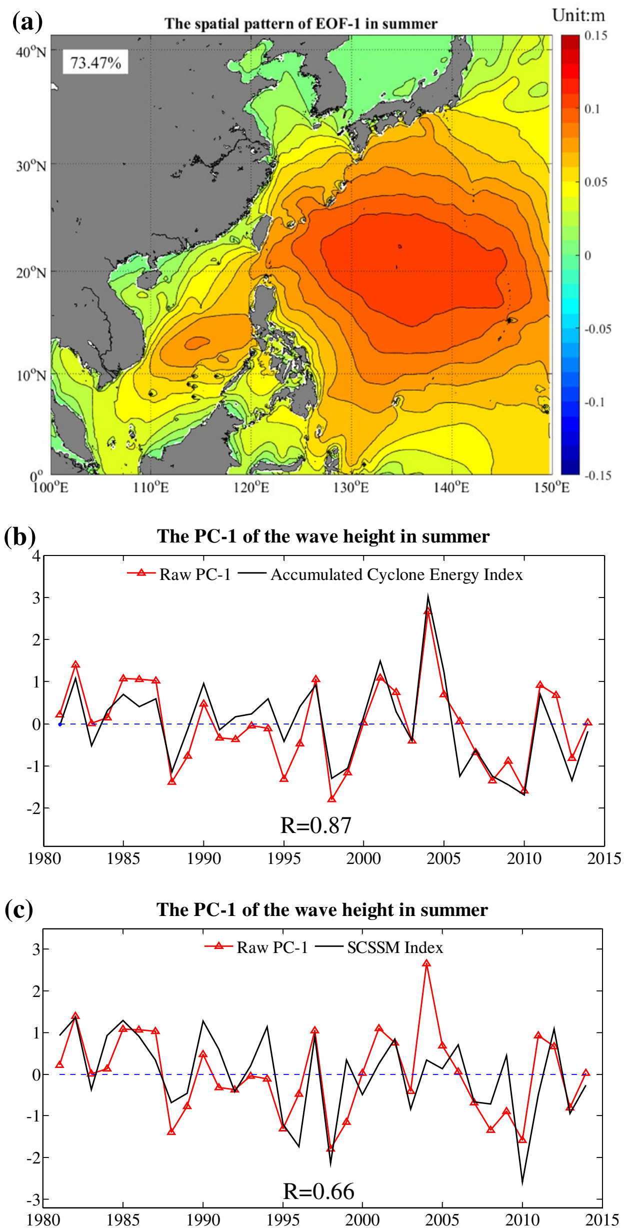

Fig. 10 **a** The spatial pattern and **b**, **c** corresponding principle components of the first mode of the significant wave height anomalies, overlaid with the Accumulated Cyclone Energy (ACE) index and South China Sea Summer monsoon (SCSSM) index in the WNP-SCS region in summer (JJA). All the time series are normalized. The contour level is 0.01 m in **a**

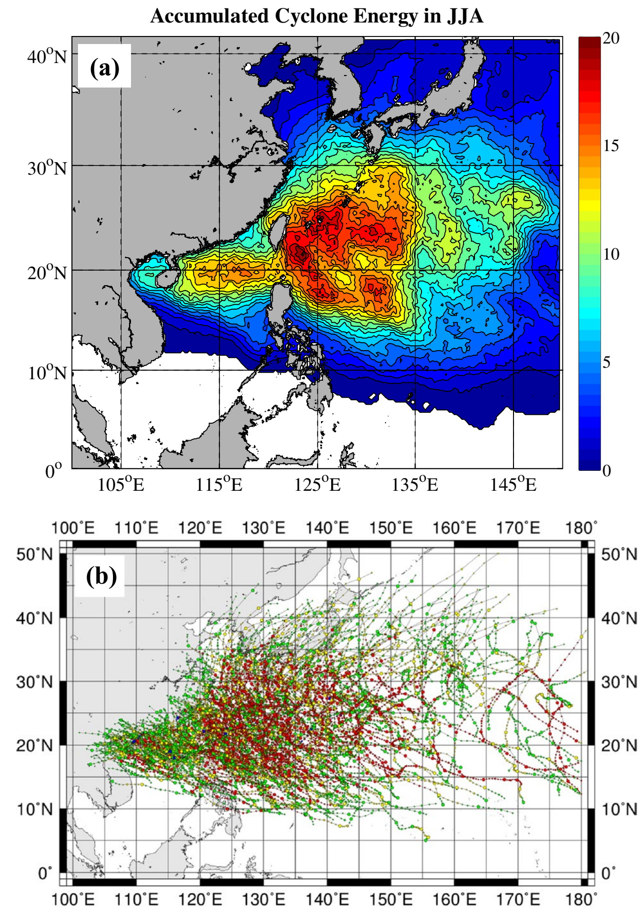

Fig. 11 **a** The summation of the accumulated cyclone energy (ACE, unit: 10^4 kn^2) averaged in summer (JJA) and **b** the tracks of 382 tropical cyclones in summer (JJA) obtained from Japan Meteorological Agency (JMA) in the WNP-SCS region during the period of 1981–2014. Saffir-Simpson Scale is used to classify the intensity of tropical storms based on the maximum sustained wind (1-min mean) in **b**. Blue: Tropical Depression (Class 2); Green: Tropical Storm (Class 3); Yellow: Severe Tropical Storm (Class 4); Red: Typhoon (Class 5); Magenta: Extratropical Cyclone (Class 6); Gray: Hurricane or Tropical Cyclone (Class 7)

tropical WNP region are mainly influenced by the TC activities in summer. Moreover, it is interesting that the REOF-1 has a significant correlation with the ONI of JJA (R = 0.66) on inter-annual time scales as well (Fig. 12c and Table 2).

The second mode of the rotated EOFs (REOF-2) explains about 22.76% of the total variance, in which large loadings mainly lie in the central SCS and extend northeastward to Luzon Strait and even the WNP region

Table 2 Correlation coefficients between the principle components (PC-1, rotated PC-1 and rotated PC-2) and three indices (ACE, SCSSM index and ONI) in summer (JJA)

Climate indices		ACE	SCSSM index	ONI
Summer	PC-1	0.87	0.66	0.58
	Rotated PC-1	0.73	–	0.66
	Rotated PC-2	–	0.71	– 0.50 (DJF)[a]

All the coefficients exceed a 99% significance level

[A]the rotated PC-2 is compared with the mature phase of El Niño-Southern Oscillation (described by Ocean Niño Index (ONI) in winter). It also has a 1-year-lagged correlation with the annual mean ONI (R = – 0.53)

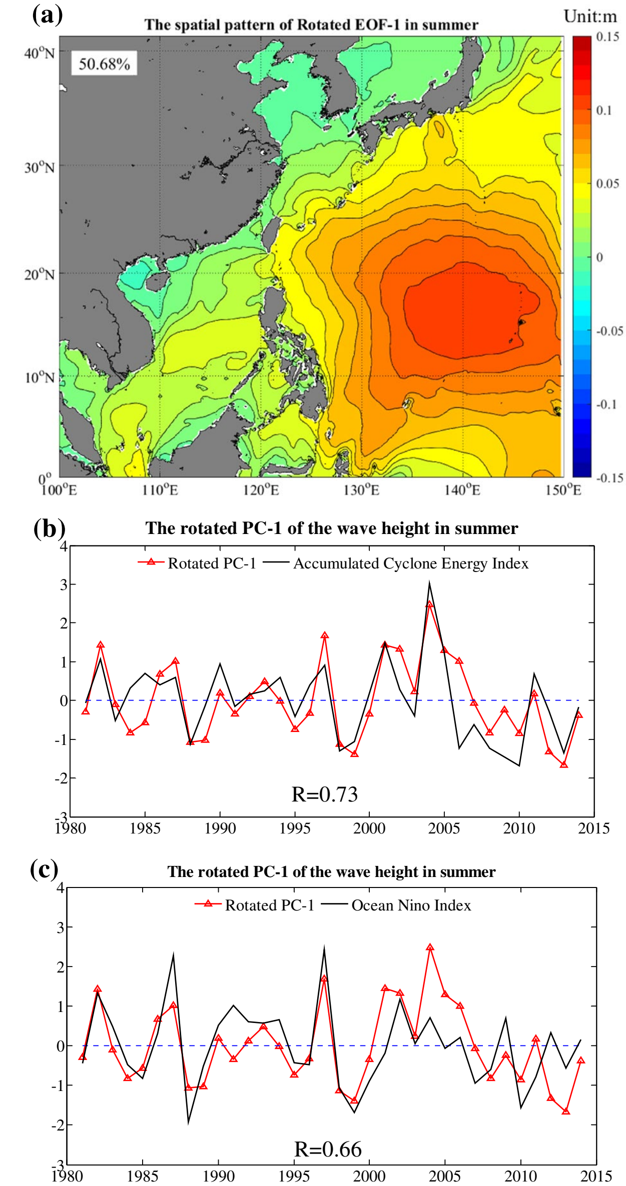

Fig. 12 **a** The spatial pattern and **b**, **c** corresponding principle components (PCs) of the first rotated mode of the significant wave height anomalies, overlaid with the Accumulated Cyclone Energy index and Ocean Niño index in the WNP-SCS region in summer (JJA). All the time series are normalized. The contour level is 0.01 m

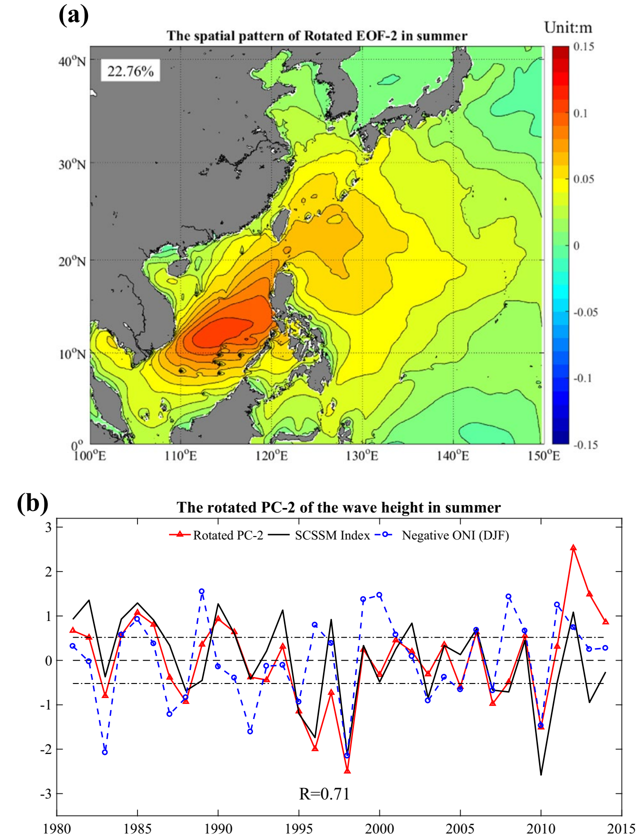

Fig. 13 **a** The spatial pattern and **b**, **c** corresponding principle components of the second rotated mode of the significant wave height anomalies (triangle marker), overlaid with the South China Sea Summer monsoon (SCSSM) index (black solid line) and negative Ocean Niño index (ONI) in winter (DJF) (circle marker), in the WNP-SCS region in summer (JJA). R = 0.71 in **b** is the correlation coefficient between the rotated PC-2 and SCSSM index; dot lines stand for ± 0.5σ of the time series of the SCSSM index. Both the time series are normalized. The contour level is 0.01 m in **a**

(Fig. 13a). The time series of the REOF-2 (rotated PC-2) has a notable correlation with the SCSSM index (Li and Zeng 2002, 2003), whose correlation coefficient is R = 0.71 above the 99% confidence level (Fig. 13b). Five major peaks correspond well to the strong SCSSM years in 1982, 1985, 1990, 2006 and 2012, while several troughs occur along with the weak SCSSM in the years of 1988, 1995, 1996, 1998 and 2010 (Zhang et al. 2019). Here, the threshold value ± 0.5δ is applied to define the strong or weak SCSSM (Chan 2016; Chen et al. 2014; Wang and Chan 2002). It can cover most of the strong SCSSM or weak SCSSM years in the previous studies (Fan et al. 2018; Zhang et al. 2019). The wind anomalies of the strong SCSSM years (SCSSM index > 0.5δ) (1981, 1982, 1984, 1985, 1986, 1990, 1991, 1994, 1997, 2002, 2006 and 2012) and the weak SCSSM years (SCSSM index < -0.5δ) (1988, 1995, 1996, 1998, 2003, 2005, 2007, 2008, 2010 and 2013) are presented in Fig. 14, compared to the climatological state. There are significant southwesterly anomalies in the strong SCSSM years between the equator and 15°N, but prominent northeasterly anomalies in the weak SCSSM years. The magnitude of the southwesterly anomalies is about 0.7–0.8 m/s in the strong SCSSM years, while the one of the northeasterly anomalies is 0.9–1.4 m/s. The southwesterly (northeasterly) anomalies intensify (weaken) the summer monsoon in the southern and central SCS, which leads to the above-normal (below-normal)

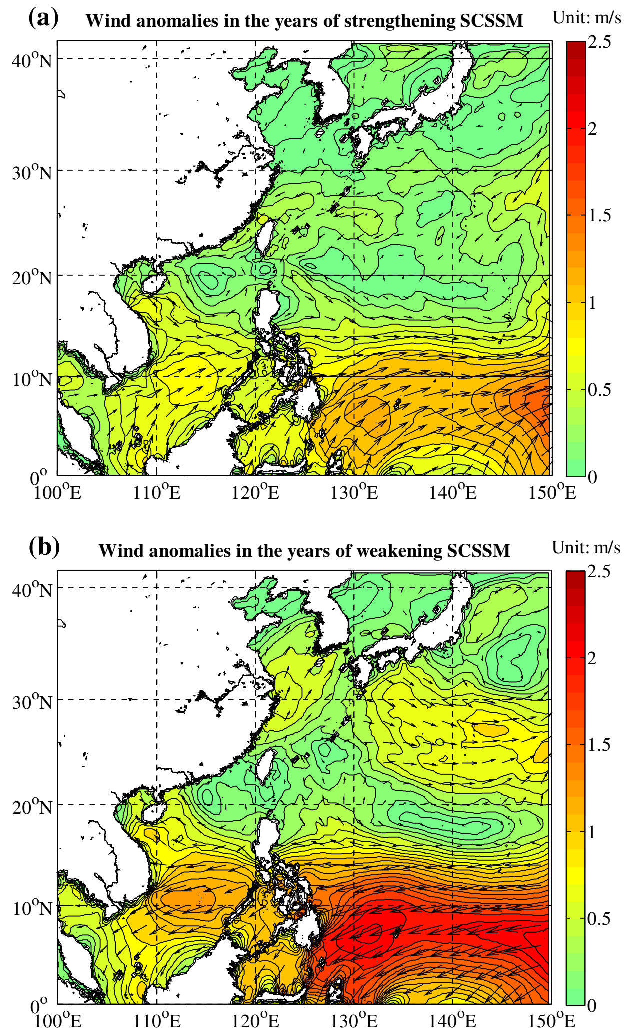

Fig. 14 Composite wind anomalies (unit: m/s) against the climatological mean in summer (JJA) of the years of **a** the strong South China Sea Summer monsoon (SCSSM) (1981, 1982, 1984, 1985, 1986, 1990, 1991, 1994, 1997, 2002, 2006 and 2012) and **b** the weak SCSSM (1988, 1995, 1996, 1998, 2003, 2007, 2008, 2010 and 2013). The contours denote the wind speed anomalies with an interval of 0.1 m/s, and the vectors are the direction of the wind anomalies

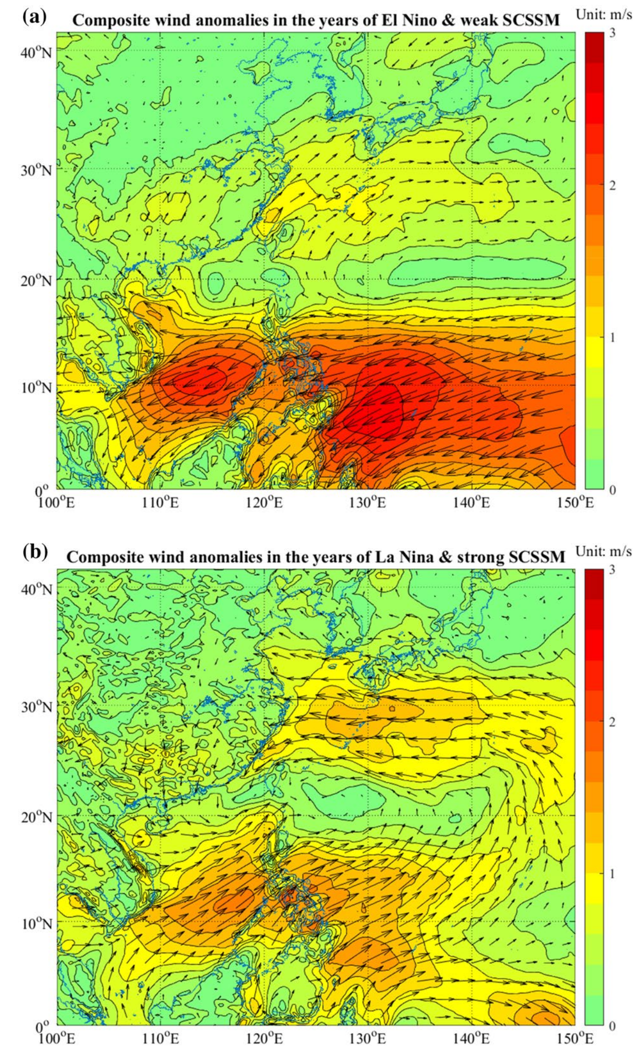

Fig. 15 Composite wind anomalies (unit: m/s) during the decaying ENSO summer (JJA) of **a** strong El Niño events with weak South China Sea Summer monsoon (SCSSM) (1988, 1995, 1998, 2003, 2007 and 2010) and **b** strong La Niña events with strong SCSSM (1985, 2006, 2009 and 2012). The contours refer to the wind speed anomalies with an interval of 0.2 m/s, and the vectors are the direction of the wind anomalies

wave height. The results indicate that the REOF-2 embodies the impact of SCSSM on the wave height in the central SCS and the region around Luzon Strait. In addition, the rotated PC-2 is found to have a notable correlation with the ONI in DJF of the preceding year ($R = -0.50$, Fig. 13b) above the 99% confidence level. As shown in Fig. 13b, the strong El Niño events in the preceding winter correspond to the trough of the SCSSM index and SWH (1988, 1995, 1998, 2003, 2007 and 2010). The composite wind anomalies in the decaying El Niño summer along with the weak SCSSM are presented in Fig. 15a. The northeasterly anomalies occur in the low-latitude WNP-SCS region, and an anomalous anticyclone exists to the east of Luzon Strait, which agrees with that in the previous works (Fan et al. 2018; Feng and Chen 2014; Wang et al. 2001). There is an opposite pattern in the years of strong SCSSM during the decaying phase of La Niña (1985, 2006, 2009 and 2012), in which the southwesterly anomalies occur in the low-latitude region with smaller magnitude than those for the decaying El Niño (Fig. 15b). The results suggest that the SWH variations in the central SCS are significantly related to the SCSSM and modulated by the decaying ENSO events.

4 Discussions

4.1 ENSO, AL and their impacts on the SWH variations in winter

4.1.1 The role of ENSO in the SWH variations in the tropical WNP

As mentioned above, an anomalous anticyclone (cyclone) over the Philippine Islands in winter during the strong El Niño (La Niña) years induces the weakening (strengthening) northeasterly monsoon and then the below-normal (above-normal) SWH in SCS and around the Philippine Islands. The connection between ENSO and the SWH over the tropical WNP in winter is illustrated by the schematic diagram in Fig. 16a. The equatorial eastern-central Pacific warming (El Niño) induces a nearby cyclone to the northwest of the warming, whose equatorward wind anomalies are superposed on the mean northeasterly trade wind. It intensifies the wind speed and the evaporation cooling in the tropical WNP. The sea surface cooling induces an anomalous anticyclone to the northwest of the cooling regions over the Philippine Sea due to a Rossby wave response to the suppressed convective heating (Gill 1980). The anomalous anticyclone develops rapidly in the late fall and persists until the following spring or early summer. In the northwest of the anticyclone, anomalous southwesterly wind prevails and suppresses the northeasterly winter monsoon, resulting in the weaker than normal SWH in the tropical WNP-SCS region. There is an opposite anomaly pattern for strong La Niña events. Besides, the magnitude of wind anomalies indicates that the impact of the warming events (El Niño) in the equatorial eastern-central Pacific is larger than that of the cooling events (La Niña).

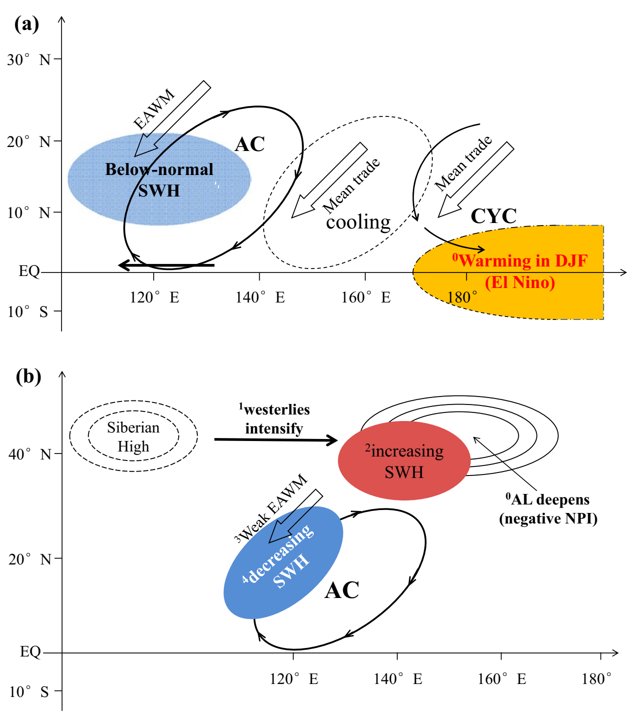

Fig. 16 Schematic diagram showing **a** the teleconnection between the warming in the equatorial eastern-central Pacific and the below-normal significant wave height (SWH) in the tropical WNP in winter (DJF), referring to Wang et al. (2000), and **b** the relationship between the Aleutian Low (AL) activities and the dipole pattern of the SWH anomalies in DJF. CYC and AC are the abbreviation of cyclone and anticyclone, respectively

Moreover, it should be noted that the warm events in 1986–1987 and 1994–1995 do not correspond to the peaks of PC-1. According to Wang et al. (2000), the strength of the equatorial eastern-central Pacific warming (the 3-month running mean Niño-3.4 SST anomalies less than 1 °C) toward the end of the ENSO development year is insufficient for the development or maintaining of the Philippine Sea anticyclone in both events.

4.1.2 The role of AL in the SWH variations in the WNP

The PC-2 of the SWH anomalies in winter is prominently correlated with the intensity variation and longitudinal shift of the AL on decadal time scales. In a strengthening (weakening) phase of the AL, the AL center shifts eastward (westward) (Sugimoto and Hanawa 2009; Wallace and Gutzler 1981). With the eastward shift of the AL center and the increasing AL intensity, the westerly wind intensifies in the subtropical WNP region (Schneider and Cornuelle 2005; Trenberth and Hurrell 1994). Meanwhile, the northeasterly monsoon weakens in the low-latitude WNP-SCS region (Chen et al. 2014; Si and Kubota 2006), along with the occurrence of the anomalous anticyclone over the Philippine Islands. As a result, the SWH is higher than normal in the region to the east of Japan, while the one in the northern SCS and east of Luzon Strait is below-normal. This process is schematically demonstrated in Fig. 16b. The wind anomalies, as well as the SWH variations, reverse in the years of weakening AL intensity.

4.2 TCs, SCSSM, ENSO and their roles on the SWH variations in summer

4.2.1 Inherent relationship among ENSO, TC activities and the SWH variations

The rotated EOF-1 of the SWH anomalies has significant correlations with the TC activities and ENSO on interannual time scales. The activities of intense TCs in WNP (described by the ACE index) is obviously impacted by the Niño-3.4 SST anomalies (Camargo and Sobel 2005; Chan

2016; Chu 2004; Wang and Chan 2002). The relationship among ENSO, TCs and SWH is illustrated by the schematic diagram in Fig. 17a and explained as follows. The warming in the equatorial eastern-central Pacific (El Niño) induces pronounced equatorial westerly anomalies in the western Pacific, which increase the low-level vorticity in the central equatorial Pacific. The increasing low-level vorticity would help spin up TCs by increasing moisture convergence and by taking potential vorticity into TCs (Wang and Chan 2002). Under this condition, the genesis locations of TCs shift eastward and equatorward, then TCs tend to have longer lifetimes and be more intense (Camargo and Sobel 2005; Wang and Chan 2002). This process imports more mechanical energy into the ocean and induces the above-normal SWH in the tropical WNP region, and vice versa for La Niña years.

4.2.2 Inherent relationship among ENSO, SCSSM and the SWH variations

The rotated EOF-2 of the SWH anomalies in summer has a prominent positive correlation with the SCSSM index as well as a significant negative correlation with the mature phase of strong El Niño (La Niña) events in DJF of the preceding years. The relationship among the decaying El Niño, SCSSM and the below-normal SWH is illustrated by the schematic diagram in Fig. 17b. During strong El Niño events, the Philippine Sea anticyclone established rapidly in late fall and develops in winter (Wang et al. 2000). Due to the positive feedback between the anticyclone and the sea surface cooling in the presence of background trade wind, the anticyclone, as well as the easterly zonal anomalies in the low-latitude WNP-SCS region, persists until the following spring or early summer accompanying with the eastward and northward shift (Fig. 15a) (Wang et al. 2000). The interaction between the atmosphere and mixing-layer ocean was proved to amplify and sustain the anomalous Philippine Sea anticyclone with the coupled GFDL AGCM-mixed-layer ocean model, prolonging the impact of ENSO on the SCSSM in the ensuing year (Lau et al. 2004; Lau and Wang 2006). Meanwhile, the Western North Pacific Subtropical High moves southward and westward in JJA (Wang et al. 2001), which contributes to the easterly wind anomalies in the low-latitude WNP-SCS region. In addition, the negative SST anomalies in WNP and positive ones in the North Indian Ocean during the decaying phase of El Niño reinforce the easterly zonal wind anomalies in the low latitude WNP-SCS region (Li et al. 2008; Wu and Li 2014; Xie et al. 2009). There is an opposite pattern in the years of strong SCSSM during the decaying phase of La Niña (1985, 2006, 2009 and 2012). Therefore, the easterly (westerly) anomalies associated with the El Niño (La Niña) peak phase in the preceding winter (Fig. 15) weaken (strengthen) the monsoon and then SWH in the central SCS in the ensuing summer.

It should be noted that some strong ENSO events do not match up well with the SCSSM, such as 1989, 1992, 1996, 2000 and 2008. Though ENSO is the major source of the SCSSM variations, there are still other influential factors which have not been identified and need further investigations (Fan et al. 2018; Feng and Chen 2014; Wang et al. 2009).

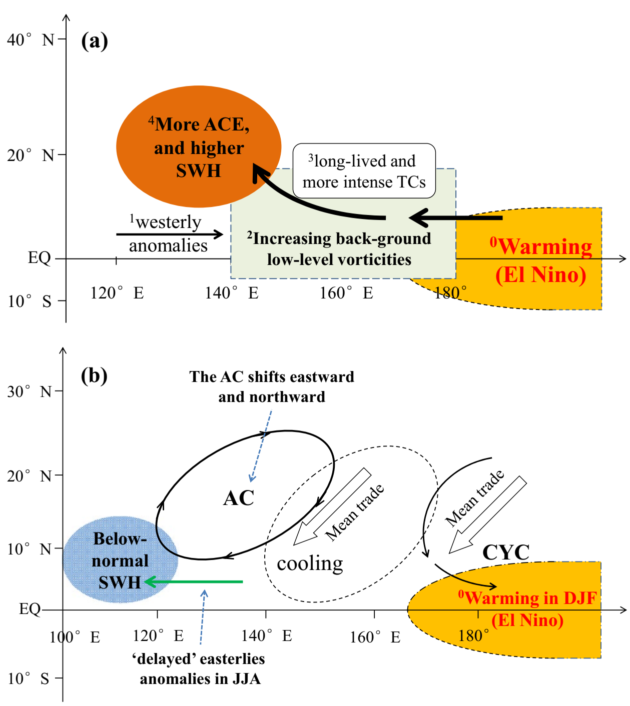

Fig. 17 Schematic diagram showing **a** the connection of El Niño events, tropical cyclone activities and the above-normal significant wave height (SWH) in the tropical WNP in summer (JJA) and **b** the relationship among the decaying El Niño, weakening South China Sea Summer Monsoon and the below-normal SWH over the central South China Sea in JJA

5 Summary

A 34-year (1981–2014) wind and wave dataset, which is produced by a coupled ocean–atmosphere model and a WAVEWATCH III model, is adopted to investigate the spatio-temporal variations of the SWH in the WNP-SCS region in winter and summer, as well as their driving mechanisms.

In terms of the annual mean, the SWH is dominated by the EAWM in the WNP-SCS region. Two regions of the high SWH occur to the east of Japan and around the Luzon Strait. The long-term trend of the SWH in the low-latitude region is slightly increasing with a phase transition in 1998, which is associated with the variation of the AL intensity or PDO.

The EOF modes of SWH anomalies are quite different in the cold and warm seasons, related to different dynamical processes. In winter, large loadings of the first mode occur in SCS and around the Philippine Islands (10° N–23° N), while the second mode shows a dipole pattern with large negative loadings in the northeastern SCS and large positive loadings to the east of Japan. The SWH variations are primarily associated with ENSO on inter-annual time scales and secondarily with the AL activities (intensity variation and longitudinal shift of the center) on decadal time scales: on one hand, the strong El Niño (La Niña) event suppresses (intensifies) the northeasterly monsoon in SCS and the east of Philippine Islands through the Philippine Sea anticyclone (cyclone), which results in the below-normal (above-normal) SWH in the tropical WNP-SCS region; on the other hand, the increasing (decreasing) AL intensity enhances (weakens) the westerly anomalies in the subtropical WNP, but weakens (enhances) the northeasterly monsoon between 15° N and 30° N, resulting in the higher (lower) SWH to the east of Japan and the lower (higher) SWH in SCS and around Luzon Straits.

In summer, the first mode has large loadings in the tropical WNP, whose time series is significantly associated with the TC activities (ACE index) in the tropical WNP and the SCSSM in the central SCS. Both TC activities and the SCSSM are influenced by ENSO. In strong El Niño years, the equatorial westerly anomalies increase the low-level vorticity in the central Pacific. Under this condition, TCs tend to have longer lifetimes and be more intense, bringing more energy to the sea surface that induces the higher SWH in the tropical WNP. In contrast, it tends to have short-lived and less intense TCs in WNP in strong La Niña years. Besides, the strong El Niño (La Niña) events in the mature phase (DJF) have a "delayed" effect on the SCSSM in the ensuing years by inducing the easterly (westerly) anomalies between the equator and 10°N, which weakens (intensifies) the SCSSM and results in the below-normal (above-normal) SWH in the central SCS.

It should be noticed that since the model domain does not cover the whole North Pacific and the model resolution is relatively low, we do not have in-depth discussions on the relationship between dynamical processes and SWH variations in this study, which will be our following work.

Acknowledgements This work was jointly supported by the National Key Research and Development Program (Grant no. 2018YFC1406206), the Major projects of the National Natural Science Foundation of China (Grant nos. 41890851 and 41931182), Guangdong Special Support Program (Grant no. 2019BT2H594), Southern Marine Science and Engineering Guangdong Laboratory (Guangzhou) (Grant no. GML2019ZD0303), the National Natural Science Foundation of China (Grant nos. 41606007, 41676016 and 41776028), Strategic Priority Research Program of the Chinese Academy of Sciences (Grant nos. XDA15020901, XDA13030103 and XDA19060503) and Chinese Academy of Sciences (Grant nos. ZDRW-XH-2019-2, ISEE2018PY05 and 133244KYSB20180029). The authors gratefully acknowledge the use of the HPCC at the South China Sea Institute of Oceanology, Chinese Academy of Sciences and the buoys observation from the National Ocean Technology Center. Thanks also to the graphic software packages, i.e., MATLAB, which were employed to plot the figures.

References

Alves J-H, Campos RM, Soares CG, Parente CE (2017) Improving surface wind databases for extreme wind-wave simulation and analysis in the South Atlantic Ocean. Clim Dyn. https://doi.org/10.7289/V5/ON-NCEP-491

Atlas R, Hoffman RN, Ardizzone J, Leidner SM, Jusem JC, Smith DK, Gombos D (2011) A cross-calibrated multiplatform ocean surface wind velocity product for meteorological and oceanographic applications. Bull Am Meteorol Soc 92:157–174. https://doi.org/10.1175/2010bams2946.1

Bell GD et al (2000) Climate assessment for 1999. Bull Am Meteorol Soc 81:S1–S50. https://doi.org/10.1175/1520-0477(2000)81[S1:Caf]2.0.Co;2

Belmonte Rivas M, Stoffelen A (2019) Characterizing ERA-Interim and ERA5 surface wind biases using ASCAT. Ocean Sci 15:831–852. https://doi.org/10.5194/os-15-831-2019

Bernstein L et al. (2008) Climate change 2007: synthesis report: an assessment of the intergovernmental panel on climate change. IPCC

Bruno MF, Molfetta MG, Totaro V, Mossa M (2020) Performance assessment of ERA5 wave data in a Swell dominated region. J Mar Sci Eng 8:214–232. https://doi.org/10.3390/jmse8030214

Caires S, Sterl A, Bidlot JR, Graham N, Swail V (2004) Intercomparison of different wind-wave reanalyses. J Clim 17:1893–1913. https://doi.org/10.1175/1520-0442(2004)017%3c1893:IODWR%3e2.0.CO;2

Camargo SJ, Sobel AH (2005) Western North Pacific tropical cyclone intensity and ENSO. J Clim 18:2996–3006. https://doi.org/10.1175/Jcli3457.1

Cavaleri L, Sclavo M (2006) The calibration of wind and wave model data in the Mediterranean Sea. Coast Eng 53:613–627. https://doi.org/10.1016/j.coastaleng.2005.12.006

Chan JCL (2000) Tropical cyclone activity over the western North Pacific associated with El Nino and La Nina events. J Clim 13:2960–2972. https://doi.org/10.1175/1520-0442(2000)013%3c2960:Tcaotw%3e2.0.Co;2

Chan JCL (2016) Interannual variations of intense typhoon activity. Tellus A Dyn Meteorol Oceanogr 59:455–460. https://doi.org/10.1111/j.1600-0870.2007.00241.x

Chen Z, Wu R, Chen W (2014) Distinguishing interannual variations of the Northern and Southern modes of the East Asian Winter Monsoon. J Clim 27:835–851. https://doi.org/10.1175/jcli-d-13-00314.1

Chu PS (2004) ENSO and tropical cyclone activity Hurricanes and Typhoons: Past, Present, and Future. Clim Dyn 2004:297–332

Craig PD, Banner ML (1994) Modeling wave-enhanced turbulence in the ocean surface layer. J Phys Oceanogr 24:2546–2559. https://doi.org/10.1175/1520-0485(1994)024%3c2546:MWETIT%3e2.0.CO;2

Fan Y, Fan K, Xu Z, Li S (2018) ENSO–South China Sea summer monsoon interaction modulated by the Atlantic Multidecadal Oscillation. J Clim 2018:31. https://doi.org/10.1175/JCLI-D-17-0448.1

Fang GH, Chen HY, Wei ZX, Wang YG, Wang XY, Li CY (2006) Trends and interannual variability of the South China Sea surface winds, surface height, and surface temperature in the

recent decade. J Geophys Res-Oceans 2006:111. https://doi.org/10.1029/2005jc003276
Feng J, Chen W (2014) Interference of the East Asian Winter monsoon in the Impact of ENSO on the East Asian Summer Monsoon in decaying phases. Adv Atmos Sci 2014:31. https://doi.org/10.1007/s00376-013-3118-8
Gill AE (1980) Some simple solutions for heat-induced tropical circulation. Q J R Meteorol Soc 106:447–462. https://doi.org/10.1002/qj.49710644905
Graham NE, Diaz HF (2001) Evidence for intensification of North Pacific winter cyclones since 1948 B Am Meteorol Soc 82:1869–1893. https://doi.org/10.1175/1520-0477(2001)082<1869:Efionp>2.3.Co;2
Hanawa K, Yoshikawa Y, Watanabe T (1989) Composite analyses of wintertime wind stress vector-fields with respect to SST anomalies in the Western North Pacific and the Enso Events Part 2. Enso composite. J Meteorol Soc Jpn 67:833–845. https://doi.org/10.2151/jmsj1965.67.5_833
Hersbach H et al (2020) The ERA5 global reanalysis. Q J R Meteorol Soc 146:1999–2049. https://doi.org/10.1002/qj.3803
Hodges K, Cobb A, Vidale PL (2017) How well are tropical cyclones represented in reanalysis datasets? J Clim 30:5243–5264. https://doi.org/10.1175/jcli-d-16-0557.1
Holland GJ (1980) An analytic model of the wind and pressure profiles in hurricanes. Mon Weather Rev 108:1212–1218. https://doi.org/10.1175/1520-0493(1980)108%3c1212:Aamotw%3e2.0.Co;2
Holthuijsen LH (2007) Description of ocean waves. In: Holthuijsen LH (ed) Waves in oceanic and coastal waters. Cambridge University Press, Cambridge, pp 24–55. https://doi.org/10.1017/CBO9780511618536.004
Jiang L, Yin Y, Cheng X, Zhang Z (2018) Interannual variability of significant wave height in the northern South China Sea. Aquat Ecosyst Health Manage 21:82–92. https://doi.org/10.1080/14634988.2017.1344455
Kalourazi MY, Siadatmousavi SM, Yeganeh-Bakhtiary A, Jose F (2020) Simulating tropical storms in the Gulf of Mexico using analytical models. Oceanologia 62:173–189. https://doi.org/10.1016/j.oceano.2019.11.001
Lau N-C, Wang B (2006) Interactions between the Asian monsoon and the El Niño/Southern Oscillation. In: Wang B (ed) The Asian Monsoon. Springer Berlin Heidelberg, Berlin, Heidelberg, pp 479–512. https://doi.org/10.1007/3-540-37722-0_12
Lau N-C, Narth MJ, Wang H (2004) Simulations By A GFDL GCM Of ENSO-related variability of the coupled atmosphere-ocean system in the east asian monsoon region. In: East Asian Monsoon, pp 271–300. https://doi.org/10.1142/9789812701411_0007
Li JP, Zeng QC (2002) A unified monsoon index. Geophys Res Lett 29:115–116. https://doi.org/10.1029/2001gl013874
Li JP, Zeng QC (2003) A new monsoon index and the geographical distribution of the global monsoons. Adv Atmos Sci 20:299–302
Li S, Lu J, Huang G, Hu K (2008) Tropical Indian Ocean basin warming and east asian summer monsoon: a multiple AGCM study. J Clim 21:6080–6088. https://doi.org/10.1175/2008jcli2433.1
Li YN, Peng SQ, Wang J, Yan J (2014) Impacts of nonbreaking wave-stirring-induced mixing on the upper ocean thermal structure and typhoon intensity in the South China Sea. J Geophys Res-Oceans 119:5052–5070. https://doi.org/10.1002/2014JC009956
Lian T, Chen DK (2012) An evaluation of rotated EOF analysis and its application to tropical pacific SST variability. J Clim 25:5361–5373. https://doi.org/10.1175/Jcli-D-11-00663.1
Lin N, Chavas D (2012) On hurricane parametric wind and applications in storm surge modeling. J Geophys Res Atmos 2012:117. https://doi.org/10.1029/2011jd017126
Liu G, Perrie W, Hughes C (2017) Surface wave effects on the wind-power input to mixed layer near-inertial motions. J Phys Oceanogr 47:1077–1093. https://doi.org/10.1175/JPO-D-16-0198.1
Luo J-J, Masson S, Behera S, Shingu S, Yamagata T (2005) Seasonal climate predictability in a coupled OAGCM using a different approach for ensemble forecasts. J Clim 18:4474–4497. https://doi.org/10.1175/jcli3526.1
Mahmoodi K, Ghassemi H, Razminia A (2019) Temporal and spatial characteristics of wave energy in the Persian Gulf based on the ERA5 reanalysis dataset. Energy 187:115991. https://doi.org/10.1016/j.energy.2019.115991
Mirzaei A, Tangang F, Juneng L, Mustapha MA, Husain ML, Akhir MF (2013) Wave climate simulation for southern region of the South China Sea. Ocean Dyn 63:961–977. https://doi.org/10.1007/s10236-013-0640-2
Monahan AH, Fyfe JC, Ambaum MHP, Stephenson DB, North GR (2009) Empirical Orthogonal functions: the medium is the message. J Clim 22:6501–6514. https://doi.org/10.1175/2009jcli3062.1
Murakami H (2014) Tropical cyclones in reanalysis data sets. Geophys Res Lett 41:2133–2141. https://doi.org/10.1002/2014gl059519
Osinowo A, Lin X, Zhao D, Wang Z (2016) Long-term variability of extreme significant wave height in the south china sea. Adv Meteorol 2016:1–21. https://doi.org/10.1155/2016/2419353
Palmer TN et al (2004) Development of a european multimodel ensemble system for seasonal-to-interannual prediction (demeter). Bull Am Meteorol Soc 85:853–872. https://doi.org/10.1175/bams-85-6-853
Pan Y, Chen Y-p, Li J-x, Ding X-l (2016) Improvement of wind field hindcasts for tropical cyclones. Water Sci Eng 9:58–66. https://doi.org/10.1016/j.wse.2016.02.002
Reistad M, Breivik Ø, Haakenstad H, Aarnes OJ, Furevik BR, Bidlot J-R (2011) A high-resolution hindcast of wind and waves for the North Sea, the Norwegian Sea, and the Barents Sea. J Geophys Res Oceans 2011:116. https://doi.org/10.1029/2010jc006402
Sasaki W, Toshiyuki H (2007) Interannual variability and predictability of summertime significant wave heights in the western north pacific. J Oceanogr 63:203–213. https://doi.org/10.1007/s10872-007-0022-9
Sasaki W, Iwasaki SI, Matsuura T, Iizuka S (2005) Recent increase in summertime extreme wave heights in the western North Pacific. Geophys Res Lett 2005:32. https://doi.org/10.1029/2005gl023722
Sasaki W, Iwasaki SI, Matsuura T, Iizuka S (2006) Quasi-decadal variability of fall extreme wave heights in the western North Pacific. Geophys Res Lett 2006:33. https://doi.org/10.1029/2006gl026094
Schneider N, Cornuelle BD (2005) The forcing of the Pacific decadal oscillation. J Clim 18:4355–4373
Semedo A, Sušelj K, Rutgersson A, Sterl A (2011) A global view on the wind sea and swell climate and variability from ERA-40. J Clim 24:1461–1479. https://doi.org/10.1175/2010jcli3718.1
Si K, Kubota M (2006) Relationship between an El niño event and the interannual variability of significant wave heights in the north pacific. Atmos Ocean 44:377–395. https://doi.org/10.3137/ao.440404
Signell RP, Carniel S, Cavaleri L, Chiggiato J, Doyle JD, Pullen J, Sclavo M (2005) Assessment of wind quality for oceanographic modelling in semi-enclosed basins. J Mar Syst 53:217–233. https://doi.org/10.1016/j.jmarsys.2004.03.006
Sugimoto S, Hanawa K (2009) Decadal and interdecadal variations of the aleutian low activity and their relation to upper oceanic variations over the north pacific. J Meteorol Soc Jpn 87:601–614
Swail VR, Cox AT (2000) On the use of NCEP-NCAR reanalysis surface marine wind fields for a long-term North Atlantic wave hindcast. J Atmos Oceanic Technol 17:532–545. https://doi.org/10.1175/1520-0426(2000)017%3c0532:otuonn%3e2.0.co;2
Tolman HL (2009) User manual and system documentation of WAVEWATCH III version 3.14 vol 166.

Trenberth KE, Hurrell JW (1994) Decadal atmosphere-ocean variations in the Pacific. Clim Dyn 9:303–319. https://doi.org/10.1007/bf00204745
Valcke S (2013) The OASIS3 coupler: a European climate modelling community software. Geosci Model Dev 6:373–388. https://doi.org/10.5194/gmd-6-373-2013
Wallace JM, Gutzler DS (1981) Teleconnections in the geopotential height field during the Northern Hemisphere Winter. Mon Weather Rev 109:784–812. https://doi.org/10.1175/1520-0493(1981)109%3c0784:TITGHF%3e2.0.CO;2
Wang B, Chan JCL (2002) How strong ENSO events affect tropical storm activity over the Western North Pacific. J Clim 15:1643–1658. https://doi.org/10.1175/1520-0442(2002)015%3c1643:Hseeat%3e2.0.Co;2
Wang XLL, Swail VR (2001) Changes of extreme wave heights in Northern Hemisphere oceans and related atmospheric circulation regimes. J Clim 14:2204–2221. https://doi.org/10.1175/1520-0442(2001)014%3c2204:coewhi%3e2.0.co;2
Wang B, Zhang Q (2002) Pacific-east Asian teleconnection Part II: How the Philippine Sea anomalous anticyclone is established during El Nino development. J Clim 15:3252–3265. https://doi.org/10.1175/1520-0442(2002)015%3c3252:Peatpi%3e2.0.Co;2
Wang B, Wu RG, Fu XH (2000) Pacific-East Asian teleconnection: how does ENSO affect East Asian climate? J Clim 13:1517–1536. https://doi.org/10.1175/1520-0442(2000)013%3c1517:Peathd%3e2.0.Co;2
Wang Y, Wang B, Oh J (2001) Impact of the preceding El Nino on the East Asian Summer atmosphere circulation. J Meteorol Soc Jpn 79:575–588. https://doi.org/10.2151/jmsj.79.575
Wang B, Huang F, Wu Z, Yang J, Fu X, Kikuchi K (2009) Multi-scale climate variability of the South China Sea monsoon: a review. Dyn Atmos Oceans 47:15–37. https://doi.org/10.1016/j.dynatmoce.2008.09.004
Wang B, Wu Z, Chang C-P, Liu J, Li J, Zhou T (2010) Another look at interannual-to-interdecadal variations of the East Asian Winter monsoon: the Northern and Southern temperature modes. J Clim 23:1495–1512. https://doi.org/10.1175/2009jcli3243.1
Wang B, Xiang B, Lee J-Y (2013) Subtropical high predictability establishes a promising way for monsoon and tropical storm predictions. Proc Natl Acad Sci 110:2718–2722
Wu X, Li S (2014) Automatic sea fog detection over Chinese adjacent oceans using Terra/MODIS data. Int J Remote Sens 35:7430–7457
Xie S-P, Hu K, Hafner J, Tokinaga H, Du Y, Huang G, Sampe T (2009) Indian ocean capacitor effect on Indo-Western Pacific Climate during the summer following El Niño. J Clim 22:730–747. https://doi.org/10.1175/2008jcli2544.1
Yan Z, Liang B, Wu G, Wang S, Li P (2020) Ultra-long return level estimation of extreme wind speed based on the deductive method. Ocean Eng 197:106900. https://doi.org/10.1016/j.oceaneng.2019.106900
Young IR (2017) A review of parametric descriptions of tropical cyclone wind-wave generation. Atmosphere 2017:8. https://doi.org/10.3390/atmos8100194
Young I, Babanin A (2020) Ocean Wave Dynamics. https://doi.org/10.1142/11509
Young IR, Zieger S, Babanin AV (2011) Global trends in wind speed and wave height. Science 332:451–455. https://doi.org/10.1126/science.1197219
Young IR, Vinoth J, Zieger S, Babanin AV (2012) Investigation of trends in extreme value wave height and wind speed. J Geophys Res Oceans 2012:117. https://doi.org/10.1029/2011jc007753
Zhang Y, Li J, Wang Q, Xue J (2019) Variations in atmospheric perturbation potential energy associated with the South China Sea summer monsoon. Clim Dyn 53:2295–2308. https://doi.org/10.1007/s00382-019-04845-7
Zheng CW, Li CY (2015) Variation of the wave energy and significant wave height in the China Sea and adjacent waters. Renew Sustain Energy Rev 43:381–387. https://doi.org/10.1016/j.rser.2014.11.001
Zheng CW, Pan J, Li JX (2013) Assessing the China Sea wind energy and wave energy resources from 1988 to 2009. Ocean Eng 65:39–48. https://doi.org/10.1016/j.oceaneng.2013.03.006
Zheng CW, Wu GX, Chen X, Wang Q, Gao ZS, Chen YG, Luo X (2019) CMIP5-Based Wave Energy Projection: Case Studies of the South China Sea and the East China Sea. IEEE Access 7:82753–82763. https://doi.org/10.1109/Access.2019.2924197
Zhu G, Lin W, Zhao S, Cao Y (2015) Spatial and temporal variation characteristics of ocean waves in the South China Sea during the boreal winter. Acta Oceanol Sin 34:23–28. https://doi.org/10.1007/s13131-015-0592-0